Nanoscale

Accepted Manuscript

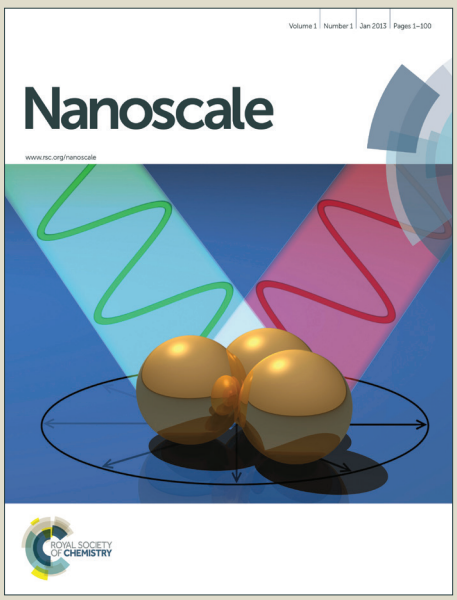

ROYAL SOCIETY OF CHEMISTRY

www.rsc.org/nanoscale

Nanoscale

RSCPublishing

ARTICLE

High Sensitivity and Wide Dynamic Range Torsion Sensors based on Graphene Woven Structure

Cite this: DOI: 10.1039/xoxxooooox

Received ooth January 2014,
Accepted ooth January 2014

DOI: 10.1039/xoxxooooox

www.rsc.org/

Tingting Yang[a,b], Yan Wang[c], Xinming Li[d], Yangyang Zhang[a], Xiao Li[a,b], Kunlin Wang[a], Dehai Wu[e], Hu Jin[f], Zhihong Li[*b,g], Hongwei Zhu[*a,b]

Due to its unique electromechanical properties, nanomaterial has become a promising material for the sensing elements of strain sensors. Tensile strain is the most well-studied deformation. Torsion is another deformation happening in daily life but has not been well understood. In the present work, a torsion sensor was prepared by wrapping graphene woven fabrics (GWFs) around a polymer rod at a fixed winding angle. The GWFs sensor showed an ultra-high sensitivity with a detection limit as low as 0.3 rad/m, indicating its potential application in highly precise measurement of low torsions. The GWFs could pre-strained before wrapped on the PDMS mode to improve tolerance of the sensor to high torsion. The microstructure of the GWFs under different torsion levels was monitored using an optical microscope. The results demonstrate the formation of GWFs waves and cracks under high torsion, which is critical to the electromechanical properties of GWFs sensor.

Introduction

Flexible sensor with user-friendly functions represents the direction for development of electronics.[1-7] It has been widely used in a variety of fields, such as human-machine interfaces, wearable electronics, real-time medical diagnostic and so on. Deformation sensor is one of well-known flexible sensors, in which sensing material can conform to arbitrarily shaped objects and transduce the deformation into accessible electrical or optical signals.[8-10] Aside from the well-studied stretching mode, others deformation modes, including compressing, shearing, twisting, vibration, torsion and bending, are also common object motions and distortions. Therefore, the development of sensors that can monitor a wide variety of complex deformations is important, theoretically and practically.

Torsion is a ubiquitous motion happening widely in daily life[11]. The steering system of vehicles, torque rod in petroleum exploration, artificial heart monitor, natural or artificial muscles and robotics are common examples of torsion. Unlike the stretching deformation that causes linear strain on an object, torsion deformation leads to normal strain and shear strain simultaneously on the surface. Thus, new demands and challenges arises to develop the sensor for torsion deformation. The current torsion sensors are based on strain gauges[12], optical fiber devices[13], acoustic wave techniques[14] and inverse magnetostrictive material[15,16]. However, most torsion sensors are complicated, rigid, high-cost and bulky. In addition, strain gauges are made with stretchable and conductive materials to record the electrical property change when the material undergoes strain. Traditional strain sensing materials, such as metal and doped semiconductor, are valid under strain level lower than 5%, indicating their relatively narrow dynamic ranges. Moreover, the gauge factors of metal and doped semiconductor are only ~2.0 and ~100, respectively. To improve the performance of torsion sensors, various new paradigms of materials with high stretchability and strain sensitivity, such as conductive polymer composites (CPCs)[17-19], evaporated metal films on stretchable polymersubstrates[20], percolating network of graphene quantum dots[21] and so on, have been developed in recent years. Hata et al. prepared a strain sensor with single-walled carbon nanotubes (SWNTs), which could withstand strains up to 280% and exhibited high durability, fast response and low creep.[22,23] However, this sensor showed a low gauge factor of 0.82 in the strain range from 0% to 40%. The gauge factor decreased to 0.06 when the strain was increased from 60% to 200%. We previously reported that graphene woven fabrics

(GWFs) coated on a polydimethylsiloxane (PDMS) substrate showed a very high strain-sensitivity with a gauge factor of 10^3 under 2 to 6% strains and the gauge factor increased to 10^6 under strains higher than 7%.[24,25] However, the material is not robust enough under strains higher than 10%, which limits its application. Therefore, the development of sensing materials with both high sensitivity and wide dynamic range remains a big challenge.

In the present work, a torsion sensor was prepared by wrapping a GWFs/PDMS strip film on a PDMS rod. A PDMS thin film was pre-stretched, followed by the deposition of chemical vapor deposited (CVD) GWFs and release of pre-stretched PDMS film. This process resulted in a buckled wave geometry of GWFs. The sensor was able to convert flattened/squeezed waves and cracks to resistance changes. The wave structure of the sensor improves its absorption of deformations and tolerance to high strain[26]. The torsion sensor with 20% PDMS thin film pre-stretched can measure and withstand torsions up to 800rad/m, which is over 8 times higher than that of conventional optical fiber torsion sensors[27] and two times higher than that of the aligned SWNTs based torsion sensor[23] with compatible sensitivity. Further increasing the pre-strain level of the PDMS thin film could result in a broader dynamic range, suggesting the potential application of this sensor as a gauge to measure high torsions. The sensor with low pre-stained PDMS film showed higher sensitivities due to the high gauge factor of GWFs. The ratio of tolerance limit of the GWFs sensor (R/R_0) with and without pre-strain reached 10^3 at 100 rad/m torsion, which is 700 times higher than that of the aligned SWNT torsion sensor[23]. The detection limit of the torsion sensor is as low as 0.3 rad/m, indicating its potential applications in ultra precise measurement of low torsions.

Results and discussion

Torsion sensors were prepared by wrapping a GWFs/PDMS strip film onto a PDMS rod with a predetermined winding angle as schematically illustrated in Fig. 1 (see Experimental Section). (i) The GWF film was deposited on a copper mesh by an atmospheric pressure chemical vapor deposition (CVD) as our previous reports[24,25], etched with aqueous $FeCl_3$/HCl solution, and eventually moved onto a 100μm thick pre-stretched PDMS strip film substrate. The pre-stretch of the PDMS thin film (Fig. 1a) is critical to engineer the wavy structural configurations of GWFs and to improve tolerance against high strains.[21, 26] (ii) The GWFs/PDMS strip film was wrapped on a PDMS rod by adding a small amount of PDMS solution between them to form a sandwich structure of PDMS thin strip/GWFs/PDMS rod. Therefore, GWFs were sealed and isolated from the air, and thus well protected from corrosion and environmental noise. The torsion sensor prepared by this process is shown in Fig. 1c.

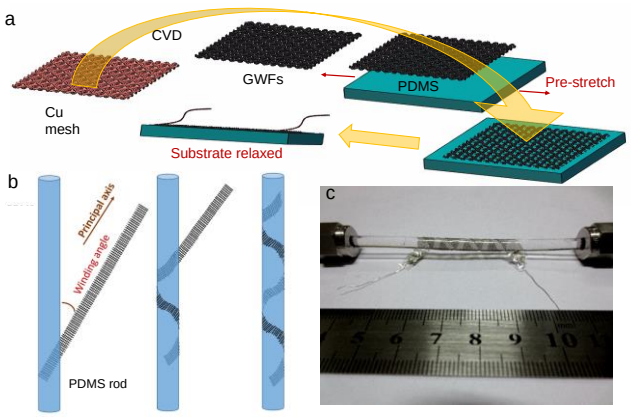

Figure 1. Preparation of GWFs-based torsion sensor. (a) Fabrication of pre-strained GWFs/PDMS film. (b) Wrapping the GWFs/PDMS film around a PDMS rod with a fixed winding angle. (c) Photograph of the assembled torsion sensor (length 7.5cm, Φ4mm).

The surface of the GWF film was characterized using a microscopy and scanning electron microscopy (SEM). Only random micro-cracks and wrinkles were found in the GWFs deposited on 0% pre-strained PDMS film (Fig. S1a and S1b). On the contrary, the GWFs film deposited on a 10% pre-strained PDMS film showed highly organized parallel waves with vector in the pre-strain direction, e.g. principal axis direction. When pre-stretch is released, the PDMS thin film contracts in the principal axis direction and expands in the vertical direction due to the Possion effect. In consequence, the GWFs film subjects to compressive stress in the principal direction and tensile stress in the vertical direction simultaneously. Thus buckled waves in the principal axis direction and a number of cracks parallel to the principal axis were found on the surface of the GWFs film. The morphology of the GWFs film on the copper mesh were further investigated with an SEM. The surface of copper wires in the mesh are very rough due to the surface reconstruction by high-temperature annealing. Graphene domains were formed on the surface the upper copper wires by a three-step growth process including multilayer island nucleation, island growth and interconnection into a film. Thereafter, a GWFs film comprising of a patchwork of graphene mosaic was covered on the copper surface and the junction points between the upper and lower copper wires (Figs. S2d and S2e). After the copper was etched and the GWFs film was transferred onto the PDMS substrate, the upper and lower part of the pipe wall of GWFs remained its original shape under the influence of the tension itself and substrate restriction, proned to collapse and crumple and resulted in irregular wrinkles (Fig. S2a). Our previous work[24,25] demonstrated that GWFs film grown on copper meshes was 4~10 layers polycrystalline.[24,25] The AFM image of the side the graphene micron-micron indicates that it is 3~7 nm thick due to the presence of surface wrinkles and graphene domain overlaps (Fig. S3).

The produced wave is vitally important in improving the stretchability of the GWFs film because the GWFs can be stretched to flat while its internal conducting network structure not being destroyed. In addition, the buckled wave structure can

be engineered by simply adjusting the pre-stretch level of the PDMS thin film. Assuming the produced periodic parallel waves is sine wave, the max tensile strains (peak strain ε_{peak}) at the surfaces of the GWFs were approximately estimated by Eq.(1)[25]:

$$\varepsilon_{peak} = \frac{2\pi^2 Ah}{\lambda^2} \quad (1)$$

where A and λ are amplitude and wavelength of ordered parallel waves and h represents the thickness of GWFs. Ribbon strain of GWFs was defined as the ratio of the length of GWFs strip to the length of pre-strained GWFs strip. The absolute peak strain is much smaller than the ribbon strain of the GWFs with a similar stretchability as that in wavy nanoribbons of GaAs and Si[26]. The amplitude and wavelength of ordered parallel wave A and λ depend on the ribbon strain of GWFs as demonstrated in Eq.(2)[21]:

$$\frac{2\pi h}{\lambda} = \left(\frac{4(1-\nu_1)^2 E_2}{E_1}\right)^{\frac{1}{3}}$$
$$\frac{A}{h} = \sqrt{\frac{2}{3}\left(\frac{\varepsilon_0}{\varepsilon_c} - 1\right)} \quad (2)$$

where E_1 and E_2 are Young's moduli; ν_1 and ν_2 are Poisson's ratios of the GWFs and the PDMS film, respectively; ε_c is the critical buckling strain of the GWFs and ε_0 represents the ribbon strain of GWFs after deposition and PDMS relaxed. The ribbon strain of GWFs comply with the strain of pre-stretched PDMS thin film but might be smaller due to the low modulus of PDMS and island effects[26].

The relative resistance changes of the torsion sensors at 45° winding angle under twisting motions were recorded in Fig. 2a and Supplementary Movie 1. All sensors various pre-stretched degree give monotonic and continuous increasing curve with exponential trend at the beginning. The torsion tolerance limit was increased from 100 rad/m to 800 rad/m accompanied with reduced sensitivity when the pre-stain level was increased from 0% to 20%. The wide dynamic range of the pre-strained GWFs sensor endows its potential application as a gauge to measure torsions higher than 100 rad/m. Moreover, wider dynamic range could be obtained with higher pre-stretch degree of the PDMS thin film. Meanwhile, the GWFs sensor with 0% pre-strech showed high sensitivity due to its high gauge factor. Thus it can be applied to the precise measurement of low torsion. For example, the performance of a torsion sensor with 0% pre-stretched PDMS was determined by monitoring its relative resistance change under low torsion level repeated for 6 torsion cycles (Fig. 2 and Supplementary Movie 2). The sensor is able to distinguish 0.3 rad/m torsion from environmental noise. When torsion was applied in the opposite direction, the resistance was also increased but with lower sensitivity than that for forward torsion (Fig. 2c). Thus, the torsion sensor cannot discriminate forward and opposite torsion merely by its resistance change. Fig. 2d is the photographs of the GWFs torsion sensor in the whole torsion range. Rod buckling occurred under high torsion due to the stress concentrated on the PDMS rod, restraining the increase of torsion tolerance. Tailoring the material and increasing its radius can prevent the strain-induced buckling and improve torsion tolerance[23]. In all, desired tolerance range and sensitivity can be achieved by simply adjusting the pre-stretch degree of PDMS thin film.

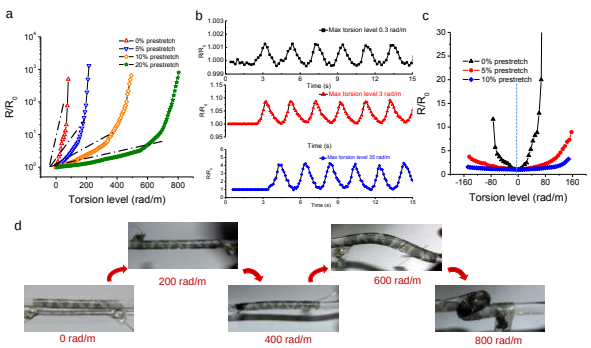

Figure 2. Electrical response characteristics of the pre-strained GWFs based torsion sensors. (a) Torsion sensor (winding angle: 45°) showing engineered combination of dynamic response range and sensitivity with various pre-strains of GWFs. (b) Relative resistance changes of the torsion sensor (winding angle: 45°) under low torsion level for 6 torsion cycles, (c) Relative changes in resistance of the torsion sensor (winding angle: 45°) under forward and opposite torsion. (d) Photographs of the torsion sensor at 0, 200, 400, 600 and 800 rad/m torsions.

As shown in our previous reported[25], GWF showed an exponential electromechanical response to stretching. The high sensitivity of the material to normal strain endow its potential application in supercapacitors[28,29], solar-cells[30], liquid sensors[31] and human motion detectors[32] . We have reported a theoretical fracture model that could be used to predicte the exponential electromechanical behavior.[25] Briefly, CVD-grown graphene has an overlapped polycrystalline structure. The adjacented graphene sheets will slide apart and then gradually break under stretching, forming cracks. The cracks hinder will cut off the current pathway. The network structure of GWFs strip is like multi-variable resistors connected in a matrix. Its high strain sensitivity can be attributed to the gradual breaking of warp and weft graphene micro-ribbons one by one under stretching. However, a torsion deformation is much more complicated than stretching. In addition, buckled waves occur in the sensor under torsion. To understand the underlying mechanism of the pre-strained GWFs torsion sensor, optical micrographs of GWFs/PDMS film with 10% pre-strain and 45° winding angle under different torsion were recorded to examine its microstructure change (Fig. 3a). Well-organized parallel buckled waves along the principal axis, as discussed above, were observed with a number of cracks parallel to the principal axis under 0 rad/m torsion. The buckled waves gradually became flat under moderate torsions, which increased the effective length of the conductor and decreased its conductivity. Meanwhile, the original cracks started closing, which increased conductivity. The former predominated the total conductivity change, resulting in an increased resistance of GWFs sensor. Interestingly, the well-organized waves perpendicular to the principal direction appeared with numerous cracks propagating primarily perpendicular to principal axis when the torsion was increased to 400rad/m (Fig. 3a). The newly-formed cracks cut off the current pathway, which dominated the conductivity change, and thus significantly increased the resistance of GWFs. When the

opposite torsion was applied, the parallel waves became squeezed and the original cracks appeared rapidly and propagated, causing the increased resistance of the sensor. These results indicate that the waves and cracks have cooperative but opposite effects on the electrical property of GWFs sensors. The waves dominate the resistance change of GWFs when few cracks appear under low torsion. The microstructure changes of GWFs conform to the theory of standard solid mechanics for the stress distribution on a solid material under torsions. The principal strains occur at ±45° relative to the long axis. GWFs bear stretching normal strain along the principal axis and compressive normal in the perpendicular direction under forward torsion with 45° winding angle as demonstrated schematically in Fig. 3b. The finite element analysis (FEA) of Mises stress on the surface of a PDMS rod indicates the stress distributes uniformly under low torsion (Fig. 3c).

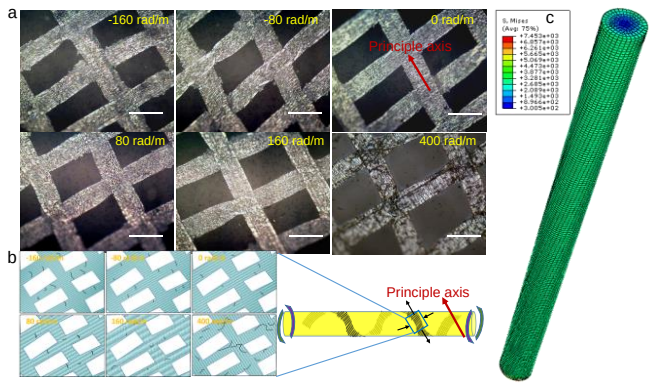

Figure 3. Microstructure of GWFs under torsions. (a) Top-view optical images under -160, -80, 0, 80, 160 and 400 rad/m torsions. Scale bars: 100μm. (b) Corresponding schematics. (c) Finite element analysis of the Mises stress distribution on the surface of a PDMS rod under low torsions.

The effect of winding angle on the performance of the sensor was also investigated in the present work. Our previous work showed that the resistance change of GWFs was primarily caused by normal tensile deformation and the change under shear strain was negligible (R/R_0<1.5 for the shear strain ranging from 0% to 50%).[25] Thus, it is predictable that the sensor with 45° winding angle has the highest sensitivity compared to the sensors with 30° and 60° winding angles. This hypothesis was confirmed with the constructed two-dimensional map (Fig. 4a). It is clear that the highest normal tensile strain in the principal axis direction is found at winding angle 45° in the whole winding angle range from 0° to 90°. Sensors with 30° and 60° winding angles have equivalent normal tensile strain and equal absolute shear strain in opposite directions, consistent with the experimental result that the both showed similar resistance-torsion behavior.

One thousand torsion cycles between 100 rad/m and 200 rad/m were performed on a GWFs sensor with 10% pre-strain and 45° winding angle. Relative resistance change versus torsion level was recorded in Fig. 4c and Supplementary Movie 3. No obvious change in the electrical properties of the GWFs sensor was observed after 1000 torsion cycles, demonstrating its stable and reliable cyclic response performances. The resistance response of GWFs sensor was also tested at 0.08, 0.4 and 2Hz change frequencies between 0 rad/m and 100 rad/m torsions. The result indicates that the pre-strained GWFs torsion sensor is non-frequency dependent in this frequency range with rapid switching at every turning point.

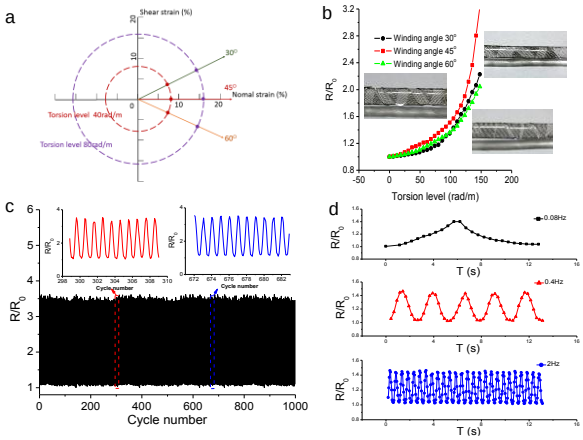

Figure 4. Electrical response characteristics of the pre-strained GWFs based torsion sensor. (a) Normal and shear strain vectors invoked by the torsion motion (red and purple dotted lines show 40 and 80 rad/m torsion level, respectively) and with 30° (green vector), 45° (red vector), and 60° (orange vector) winding angle. (b) Torsion sensor consisting of GWFs with 10% pre-strain showing dependence on winding angle. (c) 1000-cycle test showing good stability and reliability of the sensor with GWFs of 10% pre-strain and 45° winding angle under torsion level between 100 and 200 rad/m. (d) Resistance response at different frequencies for sensor with GWFs of 10% pre-strain and 45° winding angle.

Conclusions

In summary, GWFs wrapped on a PDMS rod showed wide dynamic range with appropriate pre-strains and high sensitivity without pre-strain. The pre-strain of GWFs causes ordered parallel waves, which favorites the absorption of more strains and promote its tolerance against high torsion deformation. The GWFs sensor can tolerate torsion over 8 times higher than conventional optical fiber torsion sensors and 2 times higher than the aligned SWNTs with desired sensitivity. The 20% pre-strained GWFs sensor shows comparable sensitivity with the aligned SWNTs due to the ultra-high gauge factor of pristine GWFs[25]. The ratio of tolerance limit of the GWFs sensor (R/R_0) with and without pre-strain reached 10^3 under 100rad/m torsion, which is 700 times higher than that of aligned SWNTs[23]. Additionally, GWFs is sealed by PDMS thin film and rob and isolated from environmental interferences, ensuring stable and reliable measurement. Therefore, the GWFs-based torsion sensor is able to monitor torsions as low as 0.3 rad/m due to the high gauge factor of GWFs and PDMS protection, suggesting its potential application in precise detection of ultra-low torsions. Furthermore, the pre-strained GWFs-based sensor is small and lightweight, which can be easily prepared and mounted on or embedded in other structural components. These advantages make the torsion sensor a promising candidate in a large variety

of applications such as health care, robots, recreation, industrial production, automotive electronics, virtual reality and so on.

Experimental

CVD synthesis of GWFs. Copper meshes instead of copper foils were used as the substrates for the synthesis of GWFs by atmospheric pressure CVD with methane as the carbon source[24,33]. In detail, copper meshes (100 mesh) were cleaned with hydrochloric acid solution, ethanol and deionized water. After drying with nitrogen, the copper meshes were placed in the middle of a CVD tube furnace. GWFs were synthesized at 1000°C under an $Ar/H_2/CH_4$ (200/20/15 mL min^{-1}) flow. After 15min reaction, the meshes were rapidly cooled down to room temperature under argon flow. Similar to graphene films grown on copper foil, GWFs grown on copper meshes were also polycrystalline and few-layered.

Transfer of GWFs. PDMS solution with a mass ratio (10:1) of main agent and solidification agent was spin-coated on the flat glass plank, then solidified under 80 °C for 3h. By controlling the time and rate of spin-coating (1000 rpm, 1 min), a fixed thickness of PDMS thin film (100μm) was obtained. Then GWFs on copper mesh were put into $FeCl_3$/HCl solution (1:1, mol/L) for 3h to dissolve the copper completely. A GWFs film (10 ×10cm^2) was collected with the pre-stretched PDMS film as follows: (i) the pre-stretched PDMS thin film was immerged in the $FeCl_3$/HCl solution and fixed, underneath floating GWFs; (ii) the etching solution was slowly sucked up with a needle affording that GWFs gradually fell onto the PDMS thin film. This method, to a certain extent, reduced cleavage resulted from the surface tension of water and ascertained the success of the large-size transfer of GWFs; (iii) Deionized water was then slowly injected to dilute the residual etching liquid and clean GWFs when GWFs detached from the PDMS thin film again; (iv) the same procedure as step (ii) was followed to successfully deposit GWFs onto the pre-stretched PDMS film and after drying, GWFs tightly adhere to the substrate due to the Van der Waals force. After pre-stretch PDMS thin film released, the GWFs/PDMS film was cut into strips (10 ×0.5cm^2) and silver adhesive was coated on the two ends to make electrical interconnection. The schematic diagram of this transfer process is illustrated in Fig. S4.

Assembly of torsion sensor. To assemble the GWFs/PDMS thin strip onto the surface of a Φ4 mm PDMS rod, a small amount of PDMS solution (a mixture of main agent and solidification agent before solidification) was applied between GWFs and the rod before gently rolling the elastomeric rod across the GWFs/PDMS strip at a predefined winding angle. Then the treated sample was put in a vacuum drying chamber at 80°C for 3h to solidify the added PDMS solution affording a whole sandwich structure of PDMS thin strip/GWFs/PDMS rod.

Test Platform. Torsion deformation was loaded by a series of direct current electromotor (37JB38S, 24V, 30rpm, 50rpm and 300rpm). The direct current electromotor was connected to a direct current source (ATTEN APS3003DM) or to a square wave signal provided by signal generator ATTEN ATF20B when doing frequency or cyclic tests. The electrical response of the torsion sensor was real-time recorded by Keithley 4200-SCS.

Characterizations. The microstructure of GWFs was characterized using optical microscope (ZEISS AXIO Scope.A1), scanning electron microscope (SEM, LEO1530, 10 kV) and atomic force microscope (AFM, Agilent 5100).

Acknowledgements

This work was supported by Beijing Science and Technology Program (No. D141100000514001), and National Science Foundation of China (Nos. 51372133 and 91323304).

Electronic Supplementary Information (ESI) available. See DOI: xxx.xxx.

Notes and References

[a]School of Materials Science and Engineering, State Key Laboratory of New Ceramics and Fine Processing, Key Laboratory of Materials Processing Technology of MOE, Tsinghua University, Beijing 100084, China. Email: hongweizhu@tsinghua.edu.cn

[b]Center for Nano and Micro Mechanics, Tsinghua University, Beijing 100084, China

[c]Department of Physics, Nanoscience and Nanotechnology Laboratory, Institute for Advanced Study, Nanchang University, Nanchang 330031, China

[d]National Center for Nanoscience and Technology, Zhongguancun, Beijing 100190, China

[e]Department of Mechanical Engineering, Tsinghua University, Beijing 100084, China

[f]2D Carbon Graphene Material Co., Ltd., Changzhou, Jiangsu 213149, China

[g]National Key Laboratory of Science and Technology on Micro/Nano Fabrication, Institute of Microelectronics, Peking University, Beijing 100871, China. Email: zhhli@pku.edu.cn

1 D.H. Kim, N. Lu, R. Ma, Y.S. Kim, R.H. Kim, S. Wang, J. Wu, S.M. Won, H. Tao, A. Islam, K.J. Yu, T.I. Kim, R. Chowdhury, M. Ying, L. Xu, M. Li, H.J. Chung, H. Keum, M. McCormick, P. Liu, Y.W. Zhang, F.G. Omenetto, Y. Huang, T. Coleman, J.A. Rogers, *Science*, 2011, **333**, 838.

2 M.L. Hammock, A. Chortos, B.C. Tee, J.B. Tok, Z. Bao, *Advanced materials*, 2013, **25**, 5997.

3 F. Axisa, P.M. Schmitt, C. Gehin, G. Delhomme, E. McAdams, A. Dittmar, Information Technology in Biomedicine, *IEEE Transactions on information technology in biomedicine*, 2005, **9**, 325.

4 C. Yu, C. Masarapu, J. Rong, B. Wei, H. Jiang, *Advanced materials*, 2009, **21**, 4793.

5 D.Y. Khang, H. Jiang, Y. Huang, J.A. Rogers, *Science*, 2006, **311**, 208.

6 D.H. Kim, J.H. Ahn, W.M. Choi, H.S. Kim, T.H. Kim, J. Song, Y.Y. Huang, Z. Liu, C. Lu, J.A. Rogers, *Science*, 2008, **320**, 507.

7 S.K. Lee, B.J. Kim, H. Jang, S.C. Yoon, C. Lee, B.H. Hong, J.A. Rogers, J.H. Cho, J.H. Ahn, *Nano letters*, 2011, **11**, 4642.

8 T.Q. Trung, N.T. Tien, D. Kim, M. Jang, O.J. Yoon, N.-E. Lee, *Advanced Functional Materials*, 2014, **24**, 117.

9 C. Pang, G.Y. Lee, T.I. Kim, S.M. Kim, H.N. Kim, S.H. Ahn, K.Y. Suh, *Nature materials*, 2012, **11**, 795.

10 S.C. Mannsfeld, B.C. Tee, R.M. Stoltenberg, C.V. Chen, S. Barman, B.V. Muir, A.N. Sokolov, C. Reese, Z. Bao, *Nature materials*, 2010, **9**, 859.
11 A. Szychowski, *Thin-Walled Structures*, 2014, **76**, 42.
12 A. Song, J. Wu, G. Qin, W. Huang, *Measurement*, 2007, **40**, 883.
13 C.-Y. Lin, L.A. Wang, G.-W. Chern, *Journal of Lightwave Technology*, 2001, **19**, 1159.
14 L. Reindl, G. Scholl, T. Ostertag, C. Ruppel, W.-E. Bulst, F. Seifert, *1996 IEEE Ultrasonics Symposium*, 1996, 363.
15 E. Hristoforou, A. Ktena, *Journal of Magnetism and Magnetic Materials*, 2007, **316**, 372.
16 H. Wakiwaka, M. Mitamura, *Sensors and Actuators A: Physical*, 2001, **91**, 103.
17 C. Cochrane, M. Lewandowski, V. Koncar, *Sensors*, 2010, **10**, 8291.
18 C. Cochrane, V. Koncar, M. Lewandowski, C. Dufour, *Sensors*, 2007, **7**, 473.
19 H. Pang, T. Chen, G. Zhang, B. Zeng, Z.M. Li, *Materials Letters*, 2010, **64**, 2226.
20 S.P. Lacour, J. Jones, S. Wagner, T. Li, Z. Suo, *Proceedings of the IEEE*, 2005, **93**, 1459.
21 T. S. Sreeprasad, A. A. Rodriguez, J. Colston, A. Graham, E. Shishkin, V. Pallem, V. Berry, *Nano letters*, 2013, **13**, 1757.
22 T. Yamada, Y. Hayamizu, Y. Yamamoto, Y. Yomogida, A. Izadi-Najafabadi, D.N. Futaba, K. Hata, *Nature nanotechnology*, 2011, **6**, 296.
23 T. Yamada, Y. Yamamoto, Y. Hayamizu, A. Sekiguchi, H. Tanaka, K. Kobashi, D.N. Futaba, K. Hata, *ACS nano*, 2013, **7**, 3177.
24 X. Li, P. Sun, L. Fan, M. Zhu, K. Wang, M. Zhong, J. Wei, D. Wu, Y. Cheng, H. Zhu, *Scientific reports*, 2012, **2**, 395.
25 X. Li, R. Zhang, W. Yu, K. Wang, J. Wei, D. Wu, A. Cao, Z. Li, Y. Cheng, Q. Zheng, R.S. Ruoff, H. Zhu, *Scientific reports*, 2012, **2**, 870.
26 Y. Sun, J.A. Rogers, *Journal of Materials Chemistry*, 2007, **17**, 832.
27 L. Shi, T. Zhu, Y.-e. Fan, K.S. Chiang, Y. Rao, *Optics Communications*, 2011, **284**, 5299.
28 X. Zang, Q. Chen, P. Li, Y. He, X. Li, M. Zhu, X. Li, K. Wang, M. Zhong, D. Wu, H. Zhu, *Small*, 2014, **10**, 2583.
29 X. Li, X. Zang, Z. Li, X. Li, P. Li, P. Sun, X. Lee, R. Zhang, Z. Huang, K. Wang, D. Wu, F. Kang, H. Zhu, *Advanced Functional Materials*, 2013, **23**, 4862.
30 X. Li, X. Zang, X. Li, M. Zhu, Q. Chen, K. Wang, M. Zhong, J. Wei, D. Wu, H. Zhu, *Advanced Energy Materials*, 2014, doi: 10.1002/aenm.201400224.
31 T. Yang, H. Zhang, Y. Wang, X. Li, K. Wang, J. Wei, D. Wu, Z. Li, H. Zhu, *Nano research*, 2014, doi: 10.1007/s12274-014-0448-5.
32 Y. Wang, L. Wang, T. Yang, X. Li, X. Zang, M. Zhu, K. Wang, D. Wu, H. Zhu, *Advanced Function Materials*, 2014, doi: 10.1002/adfm.201400379
33 X. Li, H. Zhu, K. Wang, A. Cao, J. Wei, C. Li, Y. Jia, Z. Li, X. Li, D. Wu, *Advanced materials*, 2010, **22**, 2743.

